

Design of Focused Ultrasound Phased Arrays for Prostate Treatment

J. S. Tan¹, L. A. Frizzell¹, N.T. Sanghvi², R. Seip², J.S. Wu², J. T. Kouzmanoff³

¹Bioacoustics Research Laboratory, ²Focus Surgery, Inc., ³Labthermics Technologies, Inc.

Abstract— The design of phased arrays for transrectal ultrasound therapy of the prostate presents significant challenges due to anatomical constraints on the size and shape of the probe. To maximize the array performance under these constraints, the effect of array geometry was examined theoretically. Studies were conducted on spherical segment, cylindrical, and curved cylindrical arrays. Fields were computed by dividing the array elements into many point sources. The effectiveness of various configurations was evaluated by defining a parameter, G , as the ratio of the intensity at the desired focus to the maximum intensity of any unwanted lobes.

I. INTRODUCTION

In recent years, there has been a rise in interest in the use of high intensity focused ultrasound (HIFU) for thermal therapy of the prostate [1]-[2]. In current devices, a single spherically curved transducer with a fixed focal length is employed. In this theoretical study, phased array systems were investigated in order to decrease treatment times by reducing the need for mechanical scanning, and avoiding transducer replacement and repositioning [3]. The intent was to determine an optimal phased array configuration in terms of using the fewest elements while producing acceptable ultrasonic fields and flexible focusing capability.

Transrectal application of ultrasound provides an adequate acoustic window while minimizing the amount of intervening tissue (Fig. 1). Higher frequency ultrasound can thus be applied, increasing the ultrasonic absorption coefficient to produce more efficient heating.

II. METHODS

The pressure fields were calculated using the point radiator method [4], which divides the active array surface into subelements approximating point radiators. The total pressure at a given point in the field is the sum of the complex pressures contributed

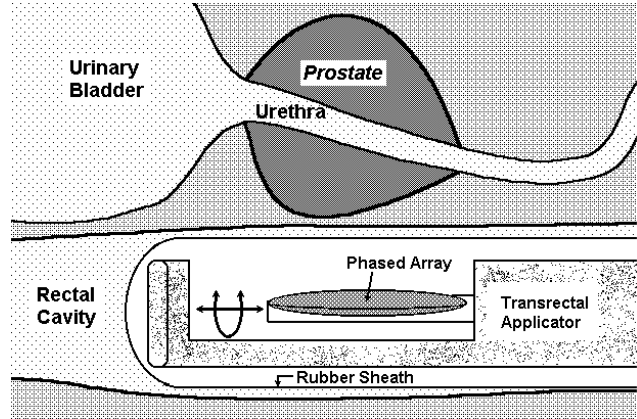


Fig. 1. Diagram of transrectal HIFU applicator

by each active subelement across the entire surface of the array, taking into account the relative phase of the signal applied to the transducer element to which the subelement belongs:

$$p(x, y, z) \cong j \frac{\rho c k U_0 \Delta A}{2\pi} \sum_{\text{array}} \frac{e^{-[\alpha_w R_w + \alpha_t R_t + jk(R_w + R_t)]}}{R_{\text{Tot}}} \quad (1)$$

where the summation is over the entire active surface of the array, $p(x, y, z)$ is the total acoustic pressure at the point (x, y, z) , ρ is the density and c is the speed of sound of the loading medium, k is the acoustic propagation constant, U_0 is the velocity amplitude of the surface of the source in m/s (calculated from $U_0 = (2I_0/\rho c)^{1/2}$, where $I_0 = 10000 \text{ W/m}^2$), ΔA is the area of the subelement, α_w is the attenuation coefficient in water, R_w is the distance that the beam traveled through water, α_t is the attenuation coefficient in tissue, R_t is the distance that the beam traveled through tissue, and $R_{\text{Tot}} = R_w + R_t$ is the total distance that the beam traveled along the straight line from source subelement to field point. The simulations were carried out at a frequency of 4 MHz.

For a given array configuration, the pressure field was calculated for the focus steered to the anticipated extremes of the treatment region, -15 mm in the y (lengthwise) or z (depth) directions. Array performance was assessed by first calculating the acoustic intensity at each field point, using the

equation $I = p^2/2\rho c$, and then finding the ratio of intensity at the focus to the intensity of the largest unwanted lobe, which was termed G:

$$G = I_{\text{focus}}/I_{\text{max,unwanted}} \quad (2)$$

Examples of calculated intensity fields are shown below in Fig. 2.

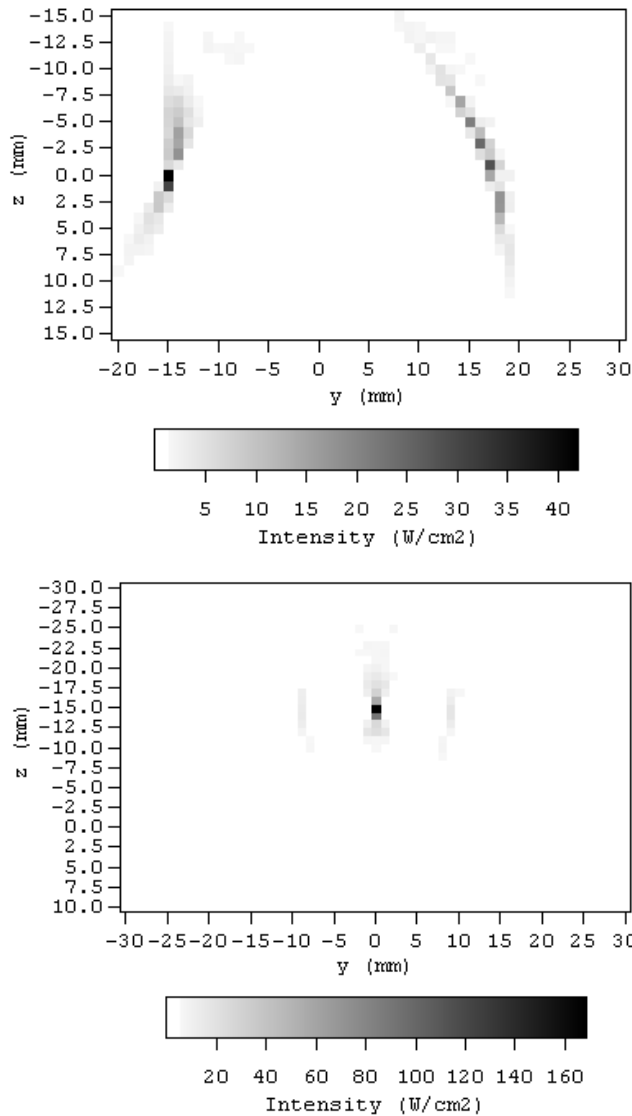


Fig. 2. Example intensity fields for arrays steered -15 mm in the y (top) and z (bottom) directions. An undesired lobe is seen in the top figure.

Truncated Spherical Annular (TSA) Array

The truncated spherical annular (TSA) array consisted of a spherical shell transducer, truncated at the sides to a width of 22 mm to allow passage into the rectal cavity and divided into annular elements with gaps ($1/2 \lambda$ wide) between annuli (Fig. 3). The

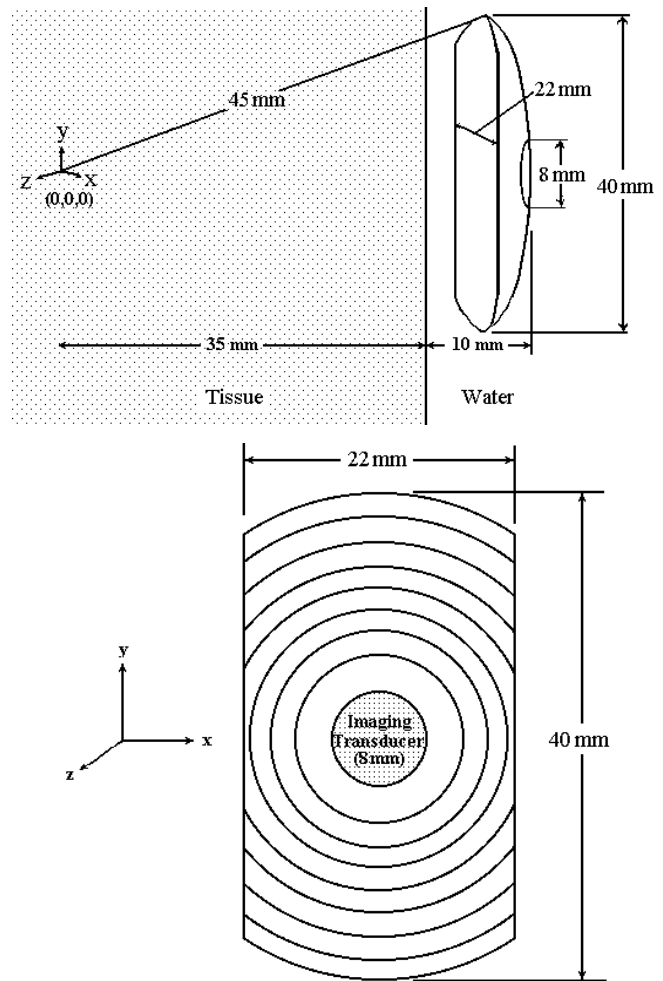


Fig 3. Side (top) and front view of TSA array.

central region of the array was left empty for an imaging transducer. A similar array configuration was previously studied by Chapelon et al. [5].

In this case, only steering of the focus in depth (z direction) was studied.

Truncated Spherical Linear (TSL) Array

The truncated spherical linear (TSL) array had an overall geometry identical to the TSA array, but with linear elements along the y direction with gaps ($1/2 \lambda$ wide) between elements (Fig. 4). Each linear element was also subdivided into 6 subelements in the x direction to improve performance. A similar array was studied by Curiel et al [6].

Cylindrical Array

The cylindrical transducer array had a width of 22 mm to allow access through the rectum, and the length was varied from 40 mm to 60 mm (Fig. 5).

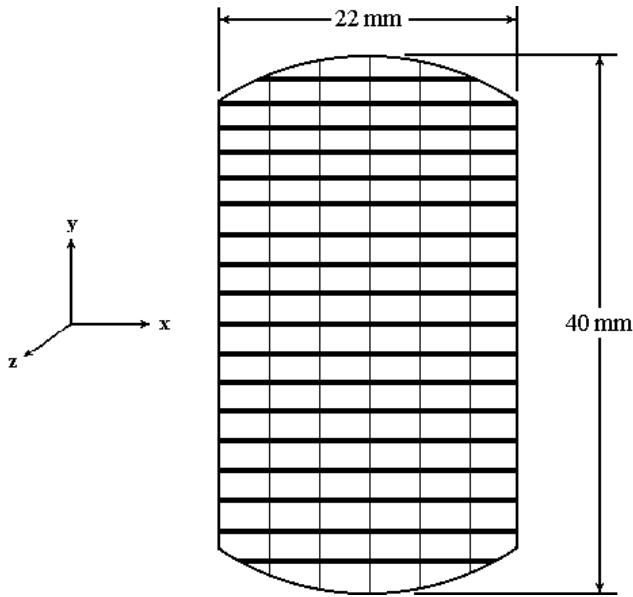


Fig. 4. Front view of TSL array.

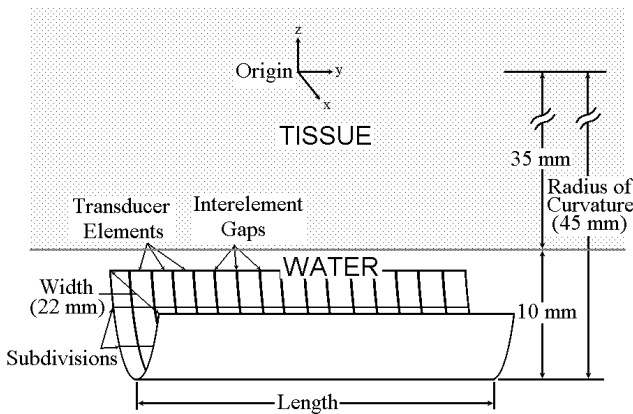


Fig. 5. Diagram of cylindrical array.

Curved Cylindrical (CC) Array

The TSL and cylindrical array configurations represented opposite extremes of a geometric and performance spectrum. The curved cylindrical array, which consisted of a cylindrical array to which a variable curvature was applied along its length, was devised in order to find a compromise that performed well when steered in both y and z directions (Fig. 6).

III. RESULTS

The simulations indicated that the performance of the TSA array when steered -15 mm in the z direction improved with increasing number of annuli (Fig. 7). The performance of the TSA array was fairly good

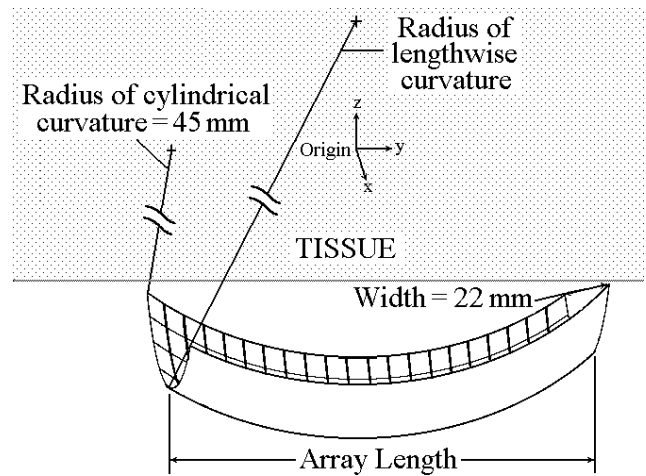


Fig. 6. Diagram of curved cylindrical array.

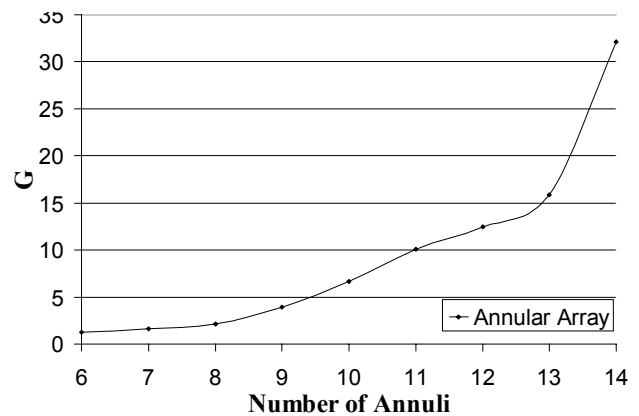


Fig. 7. G versus number of annuli for TSA array focused at $(0,0,-15)$ mm.

for arrays with as few as 10 annuli ($G > 6$). With 6 annuli, the focal intensity was roughly equal to the maximum unwanted field intensity (G value ~ 1).

For 2-dimensional electronic steering of the focus, the TSL array was initially examined. The TSL array performed well when steered 15 mm in the z (depth) direction, as seen in Fig. 8 (top), with G values above 10 even for relatively large element widths of 3λ . However, the TSL array performed relatively poorly when steered 15 mm in the y direction (parallel to the length of the rectal cavity), with most G values below 1.5, as seen in Fig. 8 (bottom). Array performance was dependent on element width in both cases, and improved with smaller element widths.

The results presented in Fig. 9 indicate that the cylindrical array performed better than the TSL array when the focus was steered 15 mm in the y direction, with G values of around 3, even for larger element widths. This performance improved with increasing

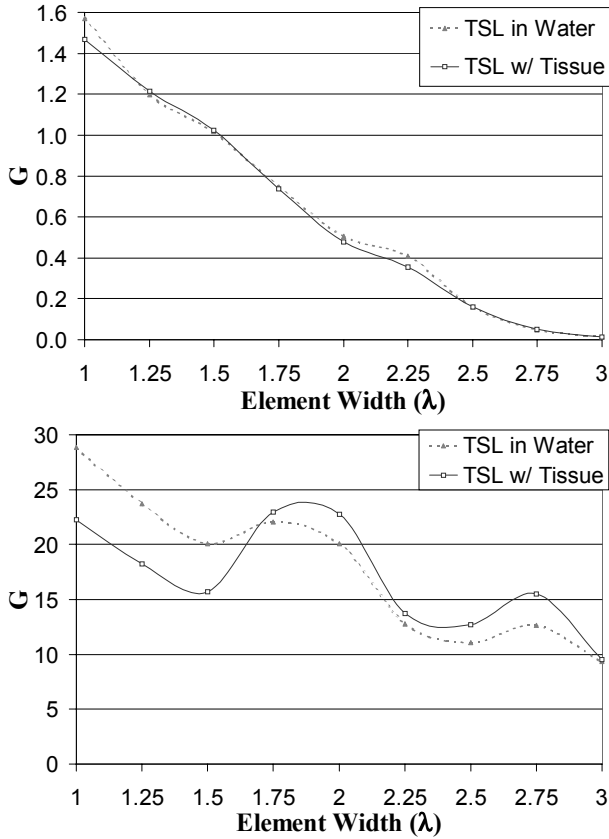


Fig. 8. G versus average element width for TSL array focused at $(0, -15, 0)$ (top) and $(0, 0, -15)$ (bottom) mm.

array length. However, when the focus was steered to $(0, 0, -15)$ mm, G values were quite low and were less than 4 for element widths greater than 1.75λ .

The performance of the curved cylindrical array was found to be intermediate between that of the TSL and cylindrical arrays. In Fig. 10, for 60 mm array lengths (solid curves) steered 15 mm in the y direction, the G values were less than 4 for element widths greater than 1.75λ . As the radius of lengthwise curvature increased, the array flattened out and the G values improved, as would be expected as the CC array became more like the cylindrical array. The shorter 50 mm CC arrays (dashed curves) were similar, with somewhat lower G values.

For steering 15 mm in the z direction, there was a slight improvement of performance with increasing array length. In this case, following the set of solid curves as an example, as the radius of lengthwise curvature increased and the array flattened out, the G values decreased.

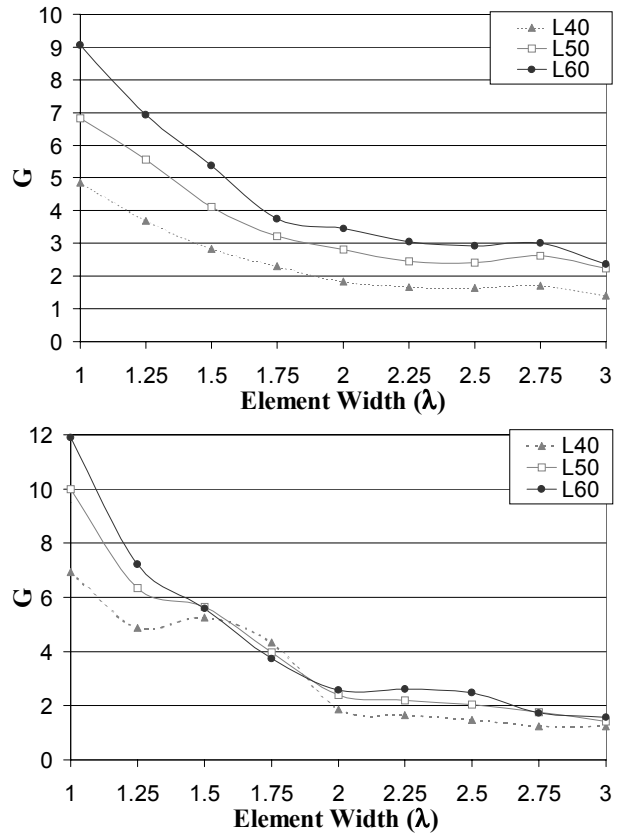


Fig. 9. G versus average element width for cylindrical array focused at $(0, -15, 0)$ (top) and $(0, 0, -15)$ (bottom) mm.

By varying the array length and the radius of lengthwise curvature, the performance of the CC array could be adjusted to achieve a compromise providing acceptable performance when steering in both the y and z directions.

IV. CONCLUSIONS

The truncated spherical annular (TSA) array was studied in order to evaluate its performance when steering -15 mm in the z direction. With as few as 10 annuli, G values above 6 were obtained. The TSA array is therefore a good candidate for electronic focusing in depth, eliminating the need to change transducers during the course of a HIFU procedure in order to vary treatment depth.

The truncated spherical linear (TSL) array was shown to allow adequate steering in the z direction. However, due to its poor performance when in the y direction, mechanical steering of the focal position

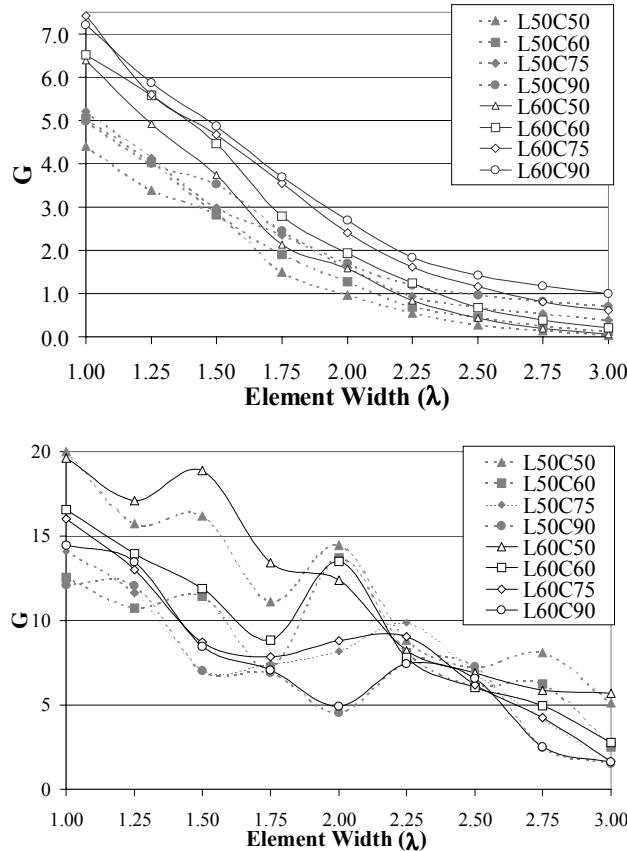


Fig. 10. G versus average element width for curved cylindrical array focused at $(0, -15, 0)$ (top) and $(0, 0, -15)$ (bottom) mm.

could not be eliminated, making it unacceptable for 2-dimensional electronic focal steering.

The cylindrical array exhibited improved steering in the y direction, relative to the TSL array. Increasing the array length array improved results for y direction steering. However, its performance when steered -15 mm in the z direction was rather poor. The cylindrical array was suitable for scanning of the focal position within a plane parallel to the rectal wall, but could not be used to change the focal depth.

The curved cylindrical (CC) array was proposed as a compromise, in order to take advantage of the best features of the spherical and cylindrical arrays. As hoped, the performance of the curved cylindrical array was between that of the truncated spherical array and the cylindrical array. Because of its variable curvature and length, the curved cylindrical array design may be optimized for steering in both the y and z directions. This array design shows excellent promise for experimental testing and possible use as a phased array for prostate treatment.

V. REFERENCES

- [1] N.T. Sanghvi, R.S. Foster, R. Bihrl, R. Casey, T. Uchida, M.H. Phillips, J. Syrus, A.V. Zaitsev, K.W. Marich, F.J. Fry, "Noninvasive surgery of prostate tissue by high intensity focused ultrasound: an updated report," *Eur. J. Ultrasound*, vol. 9, pp. 19-29, 1999.
- [2] A. Gelet, J.Y. Chapelon, R. Bouvier, C. Pangaud, Y. Lasne, "Local control of prostate cancer by transrectal high intensity focused ultrasound therapy: preliminary results," *J. Urology*, vol. 161, pp. 156-162, 1999.
- [3] E.B. Hutchinson, K. Hynynen, "Intracavitary ultrasound phased arrays for noninvasive prostate surgery," *IEEE Trans. Ultrason., Ferroelect., Freq. Contr.*, vol. 43, no. 6, pp. 1032-1042, 1996.
- [4] K.B. Ocheltree, L.A. Frizzell, "Sound field calculation for rectangular sources," *IEEE Trans. Ultrason., Ferroelect., Freq. Contr.*, vol. 36, pp. 242-248, 1989.
- [5] J.Y. Chapelon, P. Faure, M. Plantier, D. Cathignol, R. Souchon, F. Gorry, A. Gelet, "The feasibility of tissue ablation using high intensity electronically focused ultrasound," *IEEE Ultrasonics Symposium*, pp. 1211-1214, 1993.
- [6] L. Curiel, F. Chavier, R. Souchon, A. Birer, J.Y. Chapelon, "1.5D multi-elements phased array applied to High Intensity Focused Ultrasound," *IEEE Ultrasonics Symposium*, pp. 1451-1454, 1999.
- [7] J.S. Tan, L.A. Frizzell, N. Sanghvi, R. Seip, J. Kouzmanoff, "Ultrasound phased arrays for prostate treatment I: spherical configurations," *J. Acoust. Soc. Am.*, submitted.
- [8] J.S. Tan, L.A. Frizzell, N. Sanghvi, J. Wu, R. Seip, "Ultrasound phased arrays for prostate treatment II: cylindrical configurations," *J. Acoust. Soc. Am.*, submitted.

VI. ACKNOWLEDGEMENTS

The authors gratefully acknowledge the help of Rabin Pirakitti in developing the early software.

This work was supported in part by U.S. Public Health Service Grant Nos. R43 CA 81340 and T32 CA 09067, awarded by the National Cancer Institute DHHS.